Applied Catalysis B: Environmental 115–116 (2012) 314–319

Contents lists available at SciVerse ScienceDirect

Applied Catalysis B: Environmental

journal homepage: www.elsevier.com/locate/apcatb

Influence of OH-related defects on the performances of $BiPO_4$ photocatalyst for the degradation of rhodamine B

Chengsi Pan[a], Jing Xu[a], Yi Chen[b], Yongfa Zhu[a,*]

[a] *Department of Chemistry, Tsinghua University, Beijing, 100084, PR China*
[b] *Research Center of Nano-Science and Nano-Technology, Shanghai University, Shanghai, 200444, PR China*

ARTICLE INFO

Article history:
Received 7 June 2011
Received in revised form
18 December 2011
Accepted 19 December 2011
Available online 30 December 2011

Keywords:
$BiPO_4$
OH-related defects
Photocatalyst

ABSTRACT

$BiPO_4$ photocatalysts with different concentration of OH-related defects were synthesized for various hydrothermal time. The influence of the OH groups on photocatalytic activity, mineralization and degradation process of RhB was discussed in detail excluding other factors such as BET surface area and nanostructures. The defects in the lattice were observed to noticeably decrease the photocatalytic activity by forming defect levels and recombination centers. These defect levels would limit the transfer of the carriers to produce hydroxyl and super oxide radicals. Furthermore, the deethylation intermediates like *N*,*N*,*N*0-triethyl rhodamine and *N*,*N*0-diethyl rhodamine were found to accumulate in the solution when large quantities of OH-related defects were in the $BiPO_4$ lattice. While the cleavage of the whole chromophore occurred when small quantities of OH-related defects were in the $BiPO_4$ lattice. The reduction of super oxide radicals influenced by the existence of defects was demonstrated to be good for deethylation process and thus resulted in a decrease of the mineralization degree.

1. Introduction

Many *N*-containing dye pollutants like rhodamine B (RhB) are potential to yield carcinogenic aromatic amines during natural anaerobic degradation [1]. Photocatalysis technology has attracted enormous interest in cleanup of this kind of dyes because it is an inexpensive and convenient method that can totally mineralize dye molecules into H_2O and CO_2 [2,3]. Unfortunately, the activity of the widely used photocatalyst, P25(TiO_2), is not high enough to meet industrial use. Therefore, much work needs to be done in order to identify structural parameters that help to improve available photocatalysts such as particle size, surface area, particle morphology, faces exposed, acid centers, and defects. Among these parameters, defects in photocatalysts have been regarded as one of the most important impact factors on the photocatalytic activity [4].

Besides O vacancy defects, OH-related defects are also widely existing ones in semiconductors, because protons can easily purge into the crystal site of metal oxides. These defects have been well understood in the electronic industries such as Si/SiO_2 interfaces [5] and in the scaling of metal–oxide–semiconductor (MOS) devices [6], whereas they have not been related to the photocatalytic activity until recently [7–9]. As in SiO_2 which is extensively studied, OH-related defects are often resulting in the reorganization of the bonding network [5] and further cause performance degrading due to interface charging or the onset of dielectric breakdown [6]. For photocatalysts, these defects are supposed to trap carriers, and thus form a recombination center. Zou et al. reported the degradation of photocatalytic activity in $LiNbO_3$ induced by the OH-related defects [7]. These defects are supposed to exist in many lithium-contained photocatalysts due to the analogous structure between lithium ions and protons. Our group has also reported that OH-related defects as well as the nanostructures are the main factors in the $BaTa_2O_6$ and $ZnWO_4$ photocatalytic system [8,9]. Nonetheless, although some researchers have been able to correlate photocatalytic activity with OH-related defects, there are many other parameters that affect photocatalytic processes, such as surface area and nanostructures. In addition, defects caused by O vacancy are also the main defects with interference in the above metal oxide and composite metal oxide photocatalysts [10]. Thus, determining the role of OH-related defects excluding other factors is still of great interest to solve. Besides that, there have been few studies indicating a correlation between OH-related defects and mineralization or degradation process.

Nonmetal oxoacid salt photocatalysts such as $Cu_2(OH)PO_4$ [11], Bi_2SiO_5 [12], $Bi_2O_2CO_3$ [13], and Ag_3PO_4 [14], are hard to create oxygen vacancies but easy to combine with protons to form acid salts due to the nature of the oxoacid ions. As a result, not O vacancies but OH-related defects may be particularly important factors that influence their photocatalytic activity. As one of oxoacid salt photocatalysts, $BiPO_4$, discovered by our group, exhibited more

* Corresponding author. Tel.: +86 10 62783586; fax: +86 10 62787601.
E-mail addresses: zhuyf@tsinghua.edu.cn, zhuyf@chem.tsinghua.edu.cn (Y. Zhu).

0926-3373/$ – see front matter © 2012 Elsevier B.V. All rights reserved.
doi:10.1016/j.apcatb.2011.12.030

attractive activity on dye degradation than that of P25 [15]. However, the nature of OH-related defects in the photocatalyst is at present not well understood according to the above discussion.

In this work, $BiPO_4$ with different concentration of OH-related defects synthesized at various hydrothermal reaction time. OH-related defects in the lattice were demonstrated to obviously decrease the photocatalytic activity and mineralization degree of RhB due to the formation of defect levels. Moreover, these defect levels were observed to decrease the super oxide radicals' production by trapping photogenerated electrons. This change was supposed to make more RhB degradation via the deethylation process not the cleavage of the whole chromophore.

2. Experimental

2.1. Synthesis

$BiPO_4$ nanorods were synthesized through hydrothermal process. All chemicals used were analytic grade reagents without further purification. 3 mmol $Bi(NO_3)_3 \cdot 6H_2O$ and equal molar $Na_3PO_4 \cdot 12H_2O$ were put into a beaker. Then, 30 mL of distilled water was added to the beaker and magnetically stirred for 2 h at room temperature. The pH was adjusted to 1 by the addition of concentrated HNO_3 (65 wt%). The resulting precursor suspension was transferred into a 40 ml Teflon-lined stainless steel autoclave. The autoclave was sealed and maintained at 180 °C for 12 h, 24 h, 48 h, 72 h, 96 h in a digital oven, respectively, without shaking or stirring, then allowed to cool naturally to room temperature. The products were filtered off, washed several times with distilled water, and dried at 80 °C for 24 h, subsequently.

2.2. Characterization

The products were characterized by powder X-ray diffraction (XRD) on Bruker D8-advance X-ray diffractometer at 40 kV and 40 mA for monochromatized Cu Kα1 (λ = 1.5418 Å) radiation. Morphologies and structures of the prepared samples were further examined with transmission electron microscopy (TEM) by a JEM 1010 electron microscope operated at an accelerating voltage of 100 kV. HRTEM images were obtained with a JEM 2010F field emission gun transmission electron microscope operated at an accelerating voltage of 200 kV. UV–vis diffuse reflectance spectra (DRS) of the samples were measured by using Hitachi U-3010 UV–vis spectrophotometer. Total organic carbon analyzer (Multi N/C 2100, Jena) was employed for mineralization degree analysis of MB solutions. Fourier transformed infrared spectra (FTIR) were recorded on a Thermo Nicolet Avatar 370 spectrometer between 4000 and 450 cm^{-1} using KBr pellets. Background and sample spectra were obtained from 5 scans each, in air with 0.1 cm^{-1} resolution. IR absorption intensities of O—H species were determined after baseline subtraction. Before measurement, both the sample (3 mg) and KBr (0.3 g) was mixed using agate mortar and pestle under IR lamp for 20 min to remove the physical adsorption water.

2.3. Photocatalytic test

Photocatalytic activities of $BiPO_4$ were evaluated by degradation of rhodamine B (RhB) under ultraviolet light irradiation of 11 W low-pressure lamp with 254 nm. The average light intensity was 1.5 mW/cm^2. The radiant flux was measured with a power meter from Institute of Electric Light Source (Beijing). RhB solutions (200 mL, 10^{-5} mol/L) containing 0.100 g of $BiPO_4$ were put in a glass beaker. Before the light was turned on, the solution was first ultrasonicated for 10 min, and then stirred for 10 min to ensure equilibrium between the catalysts. Three milliliters of sample solution were taken at given time intervals and separated through centrifugation (4000 rpm, 10 min). The supernatants were analyzed by recording variations of the absorption band maximum (553 nm) in the UV–vis spectra of RhB using a U-3010 spectrophotometer (Hitachi). Further intermediates were determined by HPLC-MS/MS analysis with a UV detector at 550 nm. MS was performed using a Thermo Electron Corporation LTQ ion trap mass spectrometer equipped with an ESI source operated in positive or negative ion mode. The concentration of the sample was about 1×10^{-5} mol/L.

Photoelectrochemical measurements were carried out in a conventional three-electrode, single-compartment glass cell, fitted with a synthesized quartz window, using a potentiostat. The quartz electrolytic cell was filled with 0.1 M Na_2SO_4. The ITO/$BiPO_4$ electrodes served as the working electrode. The counter and the reference electrodes were platinum black wire and saturated calomel electrode, respectively. An 11 W germicidal lamp was used as the excitation light source for ultraviolet irradiation.

The super oxide radicals were estimated according to the methods from ref. [16]. 100 ml freshly 1.22×10^{-4} mol/L nitroblue tetrazolium (NBT) in 4% 2-propanol was added into 50 mg catalysts. The propanol was used as a hydroxyl consumer. The photocatalytic reaction was carried out under ultraviolet light irradiation of 11 W low-pressure lamp with 254 nm. Before the light was turned on, the solution was first ultrasonicated for 10 min, and then stirred for 30 min to ensure equilibrium between the catalysts. The supernatants were separated through centrifugation and then analyzed by recording variations of the absorption band (350 nm) in the UV–vis spectra of NBT using a U-3010 spectrophotometer (Hitachi). The detailed mechanism is shown in supporting information scheme S1.

3. Results and discussion

3.1. Physical characterization of $BiPO_4$ photocatalysts

The morphology and crystal structure of the $BiPO_4$ nanostructures were examined by the TEM, XRD and BET measurements in order to make sure the influence of nanostructures, crystallinity, and surface area on the photocatalytic activity. These results are shown in supporting information Figs. S1–S3, and summarized in Table 1. The XRD results (supporting information Fig. S1) show that the pure monoclinic phase (space group $P21/n$, JPCDS 80-0209) is finally obtained at 12 h. After 12 h the intensity of the highest peaks slightly raises as shown in Table 1, implying that their crystallinity is steadily increased with elapse of time. No obvious increasing grain sizes and the ratio of $I(2\,0\,0)/I(0\,1\,1)$ can be observed in Table 1, implying no remarkably preferring growth after 12 h. The obtained results suggest that a long hydrothermal reaction is essential to obtain pure and highly crystallized monoclinic $BiPO_4$ though it does not cause sharp change in grain sizes and preferring growth. The TEM (supporting information Figs. S2 and S3) and Table 1 show that once the precipitate is formed, the main morphology of the $BiPO_4$ is nanorods but with lots of tiny particles around them and with the hydrothermal time increasing from 12 h to 96 h, short nanorods (length <100 nm) vanishes. This suggests that the nanodots grow by the Ostwalds ripen mechanism. However, there is no appreciable change in their overall morphologies during the hydrothermal reaction. However, there is no appreciable change in their overall size during the hydrothermal reaction as shown in Table 1. Furthermore, the BET surface area of as-prepared samples (Table 1) has no order-of-magnitude changes. It is also noted that the pore volume and average pore diameters are more or less the same due to the stable structures of as-prepared $BiPO_4$. These obtained results indicate that the crystal form, morphology, surface area, and pore structure of $BiPO_4$ synthesized for various hydrothermal time may play little part in their photocatalytic reaction.

Table 1
Morphology and BET surface area of $BiPO_4$ obtained at the various hydrothermal time.

Sample	$BiPO_4$(12 h)	$BiPO_4$(24 h)	$BiPO_4$(48 h)	$BiPO_4$(72 h)	$BiPO_4$(96 h)
Morphology	Nanorods	Nanorods	Nanorods	Nanorods	Nanorods
Crystal form	Monoclinic	Monoclinic	Monoclinic	Monoclinic	Monoclinic
Crystal Size	77.5 nm	80.5 nm	82.4 nm	84.0 nm	86.1 nm
I(120)	420	500	540	560	570
I(200)/I(110)	1.22	1.29	1.28	1.23	1.25
Size (nm × nm)	(100–400) × 70	(150–400) × 75	(250–400) × 75	(300–400) × 77	(350–420) × 80
S_{BET} (m^2/g)	3.0	2.7	2.8	3.0	2.4
Pore volume (cm^3/g)	0.008	0.008	0.007	0.008	0.006
Pore diameter (nm)	11.9	11.1	12.4	13.4	10.2

3.2. The formation of OH-related defects

According to the crystalline change, the OH-related defect number may differ a lot in $BiPO_4$ samples due to the nature of phosphate, though they have similar structure parameters. These hydroxyl defects can be detected and quantitatively estimated by IR spectra. As shown in Fig. 1, the peaks around 3480 cm^{-1} and 1620 cm^{-1} are —OH stretching vibration and bending vibration, prove the presence of the OH-related defects in the $BiPO_4$ samples [17]. 1380 cm^{-1} is also an additional band of OH vibration, which is characteristic for its variety [18]. Intensities of these three peaks obviously decrease with the increase in hydrothermal time, implying that the concentration of OH-related defects becomes less and the crystals grow better. A rough estimate of C_{OH} was obtained for each sample according to ref. [19] (supporting information Fig. S4). Such an approach has also been applied by Beneventit et al. to determine the OH content in their bismuth salt samples [20]. By considering the IR absorption band, hydroxyl concentration is about 6.0×10^{18}, 3.8×10^{18}, 2.2×10^{18}, 7.4×10^{17}, and 1.7×10^{16} cm^{-3} for $BiPO_4$(12 h), $BiPO_4$(24 h), $BiPO_4$(48 h), $BiPO_4$(72 h), and $BiPO_4$(96 h), respectively. That is 0.45, 0.29, 0.16, 0.055, and 0.0013 mol% for the above samples, respectively. On the other hand, from the Raman spectra (supporting information Fig. S5), the differences of spectra in the two stretching vibration bands at 1140 and 525 cm^{-1} provide interesting information on the structural variations. It can be assigned to the vibration of $HPO_4{}^{2-}$ [21], though these peaks were overlapped by PO_4 vibration in IR spectra. Since the $BiPO_4$ was synthesized at pH 1, it is reasonable to believe that a part of OH-related defects was in the terms of $HPO_4{}^{2-}$. Otherwise, no significant change of other vibrational peaks of $PO_4{}^{3-}$ ions has been observed due to the stable crystal phase of $BiPO_4$ during the hydrothermal reaction.

Therefore, OH-related defects in $BiPO_4$ photocatalysts may be identified into two species: one is in the lattice where H^+ combined with O atom in the compounds forming $HPO_4{}^{2-}$ as discussed above; the other is in the form of the OH groups absorbed on the surface as it generally does in TiO_2 [22]. The concentration of the latter ones could be reflected by the zeta-potential of the catalysts, which is −39.2 mV, −39.0 mV, −38.9 mV, −38.5 mV, and −25.2 mV for $BiPO_4$(12 h), $BiPO_4$(24 h), $BiPO_4$(48 h), $BiPO_4$(72 h), and $BiPO_4$(96 h), respectively. This implies that except for $BiPO_4$(96 h), the surface OH groups concentration change a little, though the total OH concentration changes large. In a word, the OH-related defects in the $BiPO_4$ lattice are decreasing with the increase in time. At the same time, the number of surface OH groups merely decreases until 72 h in the hydrothermal reaction.

3.3. Effect of OH defects on photocatalytic performances and mineralization degree

The photodegradation curve of RhB catalyzed by $BiPO_4$ and apparent kinetic constants are shown in Fig. 2a. As a comparison, the RhB photodegradated by TiO_2 (P25) was also

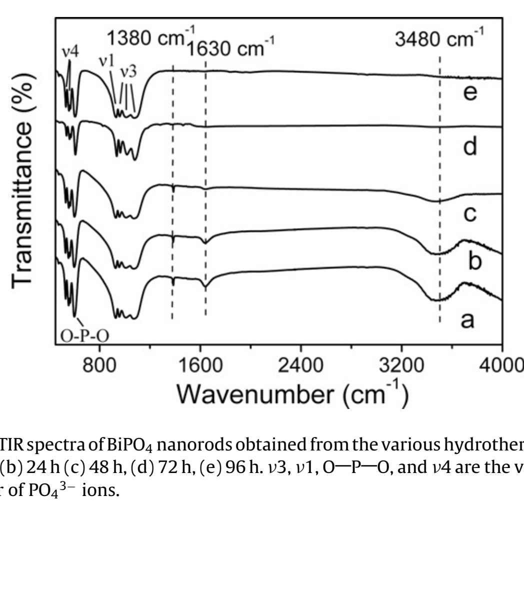

Fig. 1. FTIR spectra of $BiPO_4$ nanorods obtained from the various hydrothermal time: (a) 12 h, (b) 24 h (c) 48 h, (d) 72 h, (e) 96 h. $\nu3$, $\nu1$, O—P—O, and $\nu4$ are the vibrational behavior of $PO_4{}^{3-}$ ions.

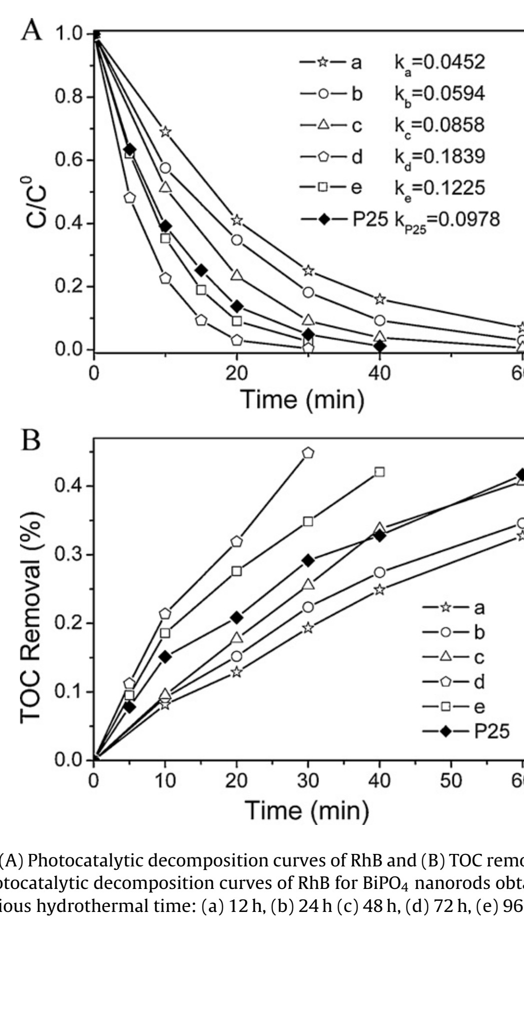

Fig. 2. (A) Photocatalytic decomposition curves of RhB and (B) TOC removal during the photocatalytic decomposition curves of RhB for $BiPO_4$ nanorods obtained from the various hydrothermal time: (a) 12 h, (b) 24 h (c) 48 h, (d) 72 h, (e) 96 h.

performed. RhB photolysis without photocatalysts could almost be neglected in the reaction time. Therefore, the ordering of the apparent kinetics of $BiPO_4$ synthesized from 12 h to 96 h is: $BiPO_4$(72 h) > $BiPO_4$(96 h) > P25 > $BiPO_4$(48 h) > $BiPO_4$(24 h) > $BiPO_4$(12 h). Clearly, photocatalytic apparent kinetic constants of $BiPO_4$(72 h) is three times more than that of $BiPO_4$(12 h) and nearly as twice as that of P25 under UV-254 illumination.

Moreover, the mineralization of dye was examined by determining the total organic carbon (TOC) in the solution, as shown in Fig. 2b. The TOC removal kinetics order is quite consistent with the RhB photodegradation activity, but the details seem to be different. After 40 min irradiation, the TOC value of the final solution is determined to be *ca.* 25–32% for P25 and $BiPO_4$(12–48 h) which suggests that deethylation dominates in the catalytic process [22]. This deethylation process is known to produce *N*,*N*,*N*$_0$-triethyl rhodamine (TER, 539 nm), *N*,*N*$_0$-diethyl rhodamine (DER, 522 nm), *N*-ethyl rhodamine (MER, 510 nm), and rhodamine at 498 nm [23]. While the TOC value of the final solution is obviously larger than 30% after 40 min irradiation for $BiPO_4$(72 h) and $BiPO_4$(96 h), that is, 45% and 35%, respectively. This shows that not only deethylation but also the cleavage of the whole chromophore structure occurs during the reaction.

For $BiPO_4$ photocatalysts, the morphology and BET surface area for the samples are almost the same (Table 1). On the contrary, OH-related defects are detected in the form of hydroxyl group by IR results. In addition, according to the nature of the nonmetal oxoacid ions, defects caused by the O vacancy is hard to yield in phosphate, that is, 5.25 eV according to Liu et al. [24] and the production of a H-related interstitial defects is about 0.5 eV [25]. For these reasons, it is reasonable to believe that OH-related defects not the O defects are the majority ones in $BiPO_4$ crystals and are one of the main factors that influences the activity and mineralization. Therefore, from 12 h to 72 h, the increasing photocatalytic activities and mineralization of the samples can be mainly attributed to the decreasing of OH defects in the lattice. With the reaction time increasing from 72 h to 96 h, the decreasing of photocatalytic activities and mineralization of the samples can be mainly attributed to the decreasing of surface OH groups which are the main source of hydroxyl radicals [22].

3.4. Effect of OH defects on the intermediates

Fig. 3a presents the characterized evolution of the spectral changes during the photodegradation of RhB on $BiPO_4$(72 h) and $BiPO_4$(12 h). In the case of $BiPO_4$(72 h) catalysts, no obvious shift of absorbance at 553 nm is observed during the photocatalytic process. On the basis of the TOC results, the diminishment of the absorption band of RhB at around 553 nm demonstrates mainly degradation of the conjugated xanthene ring in RhB on $BiPO_4$(72 h). While on $BiPO_4$(12 h), the peak changes from 554 nm to 522 nm during the discoloration process indicating the deethylation intermediates occur according to the above discussion.

To demonstrate and reveal some details of the reaction process, deethylation intermediates of RhB during the photocatalytic process were monitored by HPLC–MS–MS, and the results are displayed in Fig. 3b, supporting information Fig. S6, respectively. In the HPLC chromatogram, the peak at 10.8 min is attributed to the initial RhB, and other peaks correspond to the deethylation intermediates. It can be seen that the peak of RhB disappears quickly, and the other peaks slightly change during the degradation process on $BiPO_4$ (72 h). While for $BiPO_4$(12 h), the peak attributed to deethylation intermediates increases and then decreases. These results coincide with the spectral results.

In other words, deethylation in the RhB structure domains the degradation process when large quantities of OH defects are in the lattice. Meanwhile, the efficient cleavage of the conjugated xanthene ring in RhB occurs when small quantities of OH defects are in the lattice.

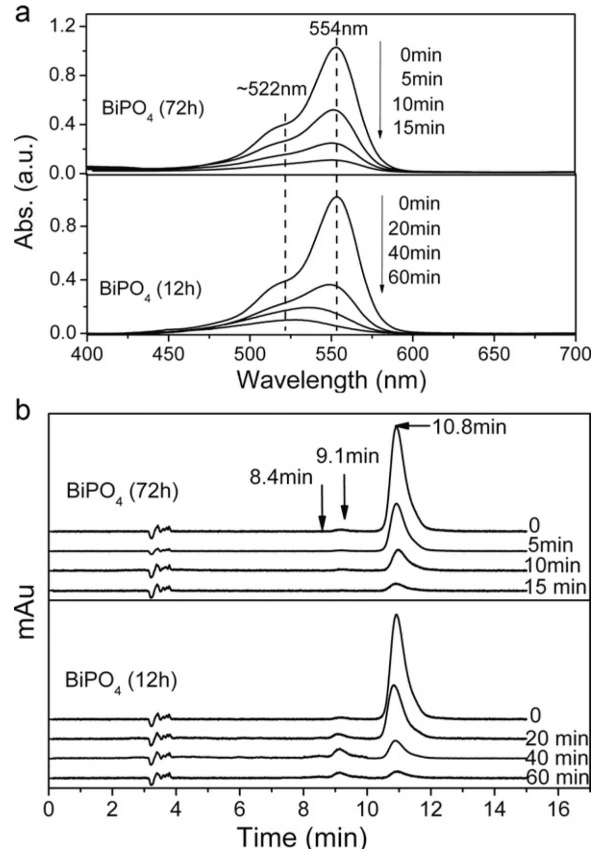

Fig. 3. (a) Temporal UV–vis absorption spectral changes for the RhB solution (10 μM) as a function of UV (254 nm) irradiation time, (b) HPLC of intermediates at different irradiation intervals on $BiPO_4$(72 h) and $BiPO_4$(12 h).

3.5. Effect of OH defects on optical absorption and photocurrent properties

The above photocatalytic activity, mineralization, and mechanism changes may be attributed to the impact of OH-related defects on intrinsic characterization of the catalysts such as the energy band position and the recombination of photoinduced e^-/h^+ pairs, which are reflected by optical absorption and photocurrent properties.

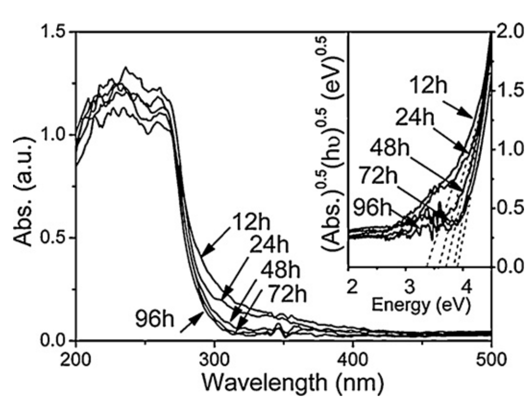

Fig. 4. UV-DRS patterns of $BiPO_4$ nanorods obtained from various hydrothermal time.

From the DRS spectra in Fig. 4, all optical absorption spectra shapes of $BiPO_4$ samples synthesized with the time increasing are almost the same, except for a little blue shift of the onset wavelength. It is more accurate for the determination of the band gap energy E_g of a semiconductor using the following equation: $\alpha = A((h\nu - E_g)^{n/2})/(h\nu)$, where α, ν, E_g, and A are absorption coefficient, light frequency, band gap, and a constant, respectively. Among them, n depends on whether the transition is direct ($n = 1$) or indirect ($n = 4$) [9]. This was due to the decrease of the defect absorption. The band gap energies estimated from the $(\text{absorbance})^{0.5} - (h\nu)^{0.5}$ versus photon energy plots (Fig. 4 inset) were 3.35, 3.60, 3.71, 3.85 and 3.88 eV for $BiPO_4$(12 h), $BiPO_4$(24 h), $BiPO_4$(48 h), $BiPO_4$(72 h), and $BiPO_4$(96 h), respectively. With the number of defects decreasing, the band gap of the samples gets larger.

In our case, the OH-related defects in the lattice are mainly caused by H^+ in the solution. The proton is in the lattice interstitial to achieve minimum formation energy, which makes the complexes of the defect type ($O_O{}^x$-$H_i{}'$-$Bi_{Bi}{}^\bullet$). This is an efficient trapping center for conduction-band electrons as reported in ZnO [26] and SiO_2 [27]. Meanwhile, the excess positive charge introduced by H^+ may be compensated by the cation vacancy ($V_{Bi}{}'''$), which leads to the formation of cation vacancy level on the valence band as described in $Ca_5(PO_4)_3OH$ and $SrTiO_3$ [28,29]. That is to say, OH-related defects not only raise the valence position but also decrease the conductive position. The change of the flat band potential can also demonstrate this conclusion (supporting information Fig. S7). It shows that compared to $BiPO_4$(72 h), the conductive band position of $BiPO_4$(12 h) is 0.30 eV lower and its valence band position raises 0.24 eV. The changes of the valence and conductive band position are known to influence the transfer of the carriers to produce hydroxyl and super oxide radicals.

The photocatalytic degradation of organic pollute can be explained as an electrochemical oxidation reaction in which reactants supply electrons to an anode. Therefore, the photogenerated current can be regarded as equivalent to the photocatalytic activity [30]. The photogenerated carriers could be easily trapped from the inner regions to the surface of the grains to take surface-mediated redox reaction [31]. So the photocurrent is considered as an indicator of the recombination rate of photogenerated e^-/h^+ pairs, as reported by Endo et al. [32]. The measured current results for $BiPO_4$(12 h), $BiPO_4$(24 h), $BiPO_4$(48 h), $BiPO_4$(72 h), and $BiPO_4$(96 h) are 14, 22, 30, 42, and 34 μA, respectively as shown Fig. 5. This result indicates under irradiation, OH defects in the lattice have the tendency to trap carriers, forming recombination centers, while the OH groups at the surface prefers to decrease surface recombination by forming $^\bullet$OH radicals.

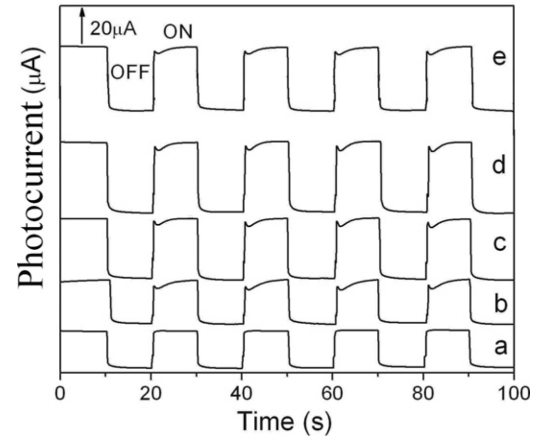

Fig. 5. Current transient with light on/off every 10 s for 100 s for $BiPO_4$ nanorods obtained at various hydrothermal time: (a) 12 h, (b) 24 h (c) 48 h, (d) 72 h, (e) 96 h.

3.6. Influence of OH-related defects on photocatalytic mechanism

With respect to the above analysis, the influence of OH-related defects in the photocatalytic reaction is shown in Fig. 6. According to the existing state, the surface OH group is good for photocatalytic reaction by forming $^\bullet$OH radicals. While the decrease of photocatalytic activity influenced by the OH-related defects in the lattice is due to the three following reasons: the first is the high concentration of them appears to prevent the irradiation released electrons reaching the Bi^{3+} centers by the broken of the Bi—O bond as they do in SiO_2 [33]; the second is they in the lattice appears to trap carriers so as to be the recombination of photogenerated e^-/h^+ pairs;

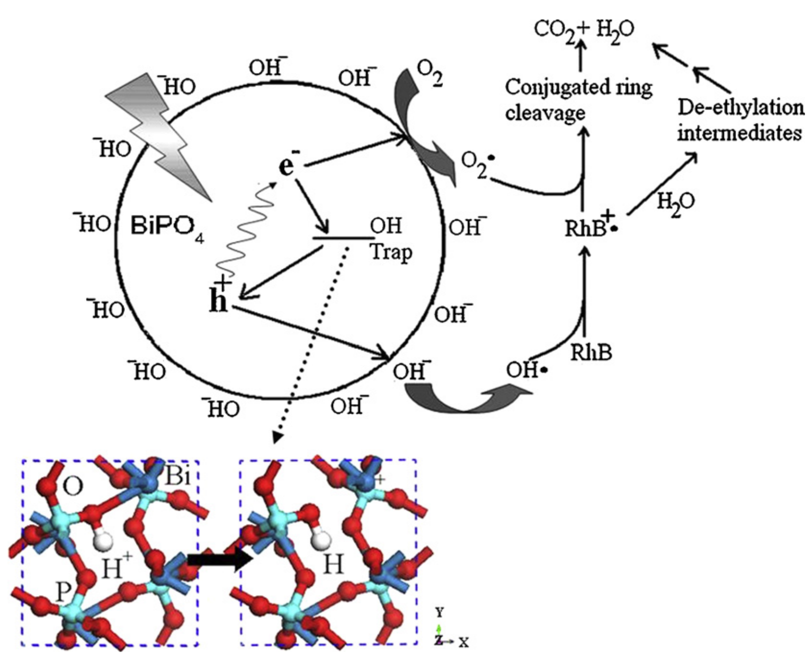

Fig. 6. Influence of the OH defects both on the photocatalytic activity and mechanism and the broking of the Bi—O bond in the $BiPO_4$ crystal.

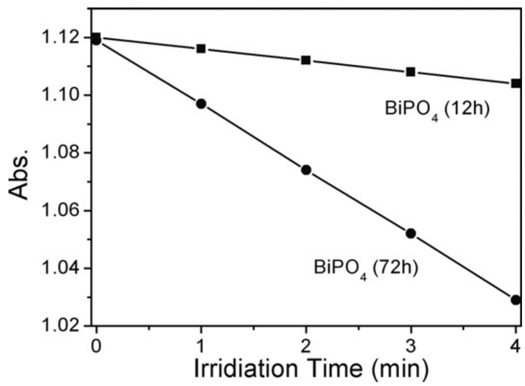

Fig. 7. The decreased intensity at 350 nm of NBT solution in the presence of $BiPO_4$(72 h) and $BiPO_4$(12 h) under UV (254 nm) irradiation time. The decreasing concentration of NBT is equal to the superoxide radical production rate.

the third one is the raise of the valence band position caused by them would limit the transfer of the holes to form hydroxyl radicals. Hydroxyl radicals are the main active groups for $BiPO_4$. [15]. In addition, after OH-related defects removal by calcination, the activity of $BiPO_4$(12 h) is very close to that of $BiPO_4$(72 h) (supporting information Fig. S8).

On the other hand, OH-related defects also influence the reaction mechanisms of RhB, also shown in Fig. 6. It is known that RhB has two selective degradation pathways: a deethylation process or a chromophore cleavage, which depends on the formation of super oxide radicals as reported by Zhao et al. [34,35]. After $RhB^{\bullet+}$ formed, the conjugated structure was broken with consuming super oxide radicals, while in the absence of super oxide radicals the deethylation process occurs due to the hydrolysis of $RhB^{\bullet+}$ radicals [34]. In our case, obvious change of super oxide radicals' production between $BiPO_4$(12 h) and $BiPO_4$(72 h) was observed, that is, 4×10^{-8} mol/min and 2.4×10^{-7} mol/min, respectively, as shown in Fig. 7. The low conductive band position due to OH-related defects is bad for the super oxide radicals' production.

4. Conclusion

In summary, $BiPO_4$ photocatalysts with different concentration of OH-related defects have been synthesized for various hydrothermal time. These OH-related defects in the lattice are demonstrated to decrease the band gap and the photocurrent, due to forming defects levels and trapping photogenerated carriers. These will further limit the transfer of the carriers to produce hydroxyl and super oxide radicals and thus decrease the photocatalytic activity. Furthermore, the reduction of super oxide radicals degraded more RhB molecules via the deethylation process not the cleavage of the whole chromophore. In addition, this study in $BiPO_4$ not only provided a way to promote its activity, but also gave a representative example for the common influence of OH-related defects in other photocatalysts for environmental pollutant degradation.

Acknowledgments

This work was partly supported by the National Natural Science Foundation of China (20925725 and 50972070), National Basic Research Program of China (2007CB613303) and Key Subject of Shanghai Municipal Education Commission (J50102).

Appendix A. Supplementary data

Supplementary data associated with this article can be found, in the online version, at doi:10.1016/j.apcatb.2011.12.030.

References

[1] A.B. dos Santos, F.J. Cervantes, J.B. van Lier, Bioresour. Technol. 98 (2007) 2369–2385.
[2] M.R. Hoffmann, S.T. Martin, W. Choi, D.W. Bahnemann, Chem. Rev. 95 (1995) 69–96.
[3] H. Fu, C. Pan, W. Yao, Y. Zhu, J. Phys. Chem. B 109 (2005) 22432–22439.
[4] X. Chen, S.S. Mao, Chem. Rev. 107 (2007) 2891–2959.
[5] M. Houssa, A. Stesmans, R.J. Carter, M.M. Heyns, Appl. Phys. Lett. 78 (2001) 3289–3291.
[6] P.E. Blöchl, J.H. Stathis, Phys. Rev. Lett. 83 (1999) 372–375.
[7] Z. Li, T. Yu, Z. Zou, J. Ye, Appl. Phys. Lett. 88 (2006) 071917.
[8] T. Xu, X. Zhao, Y. Zhu, J. Phys. Chem. B 110 (2006) 25825–25832.
[9] J. Lin, J. Lin, Y. Zhu, Inorg. Chem. 46 (2007) 8372–8378.
[10] T. Berger, M. Sterrer, O. Diwald, E. Knözinger, D. Panayotov, T.L. Thompson, J.T. Yates, J. Phys. Chem. B 109 (2005) 6061–6068.
[11] I. Cho, D.W. Kim, S. Lee, C.H. Kwak, S.T. Bae, J.H. Noh, S.H. Yoon, S.H. Jung, D.W. Kim, K.S. Hong, Adv. Funct. Mater. 18 (2008) 2154–2162.
[12] R. Chen, J. Bi, L. Wu, W. Wang, Z. Li, X. Fu, Inorg. Chem. 48 (2009) 9072–9076.
[13] Y. Zheng, F. Duan, M. Chen, Y. Xie, J. Mol. Catal. A 317 (2010) 34–40.
[14] Z. Yi, J. Ye, N. Kikugawa, T. Kato, S. Ouyang, H. Stuart-Williams, H. Yang, J. Cao, W. Luo, Z. Li, Y. Liu, R.L. Withers, Nat. Mater. 317 (2010) 559–564.
[15] C. Pan, Y. Zhu, Environ. Sci. Technol. 44 (2010) 5570–5574.
[16] H.Goto, Y. Hanada, T. Ohno, M. Matsumura, J. Catal. 25 (2004) 223–229.
[17] G. Huang, S. Zhang, T. Xu, Y. Zhu, Environ. Sci. Technol. 42 (2008) 8516–8521.
[18] H. Abbas, S.A. Nasser, J. Power Sources 58 (1996) 15–21.
[19] S. Klauer, M. Wöhlecke, S. Kapphan, Phys. Rev. B 45 (1992) 2786–2799.
[20] P. Beneventit, R. Capelletti, L. Kovács, Á. Péter, A.M.L. Manotti, F. Ugozzoli, J. Phys.: Conf. Ser. 6 (1994) 6329–6344.
[21] G.R. Sauer, W.B. Zunic, J.R. Durig, R.E. Wuthier, Calcif. Tissue Int. 54 (1994) 414–420.
[22] S. Song, Z. Liu, Z. He, A. Zhang, J. Chen, Environ. Sci. Technol. 44 (2010) 3913–3918.
[23] J. Zhuang, W. Dai, Q. Tian, Z. Li, L. Xie, J. Wang, P. Liu, X. Shi, D. Wang, Langmuir 26 (2010) 9686–9694.
[24] C.S. Liu, C.J. Hou, N. Kioussis, S.G. Demos, H.B. Radousky, Phys. Rev. B 72 (2005) 134110.
[25] K. Matsunagaw, J. Am. Ceram. Soc. 93 (2010) 1–14.
[26] W.C. Mackrodt, R.F. Stewart, J.C. Campbell, I.H. Hillie, J. Phys. Colloques 41 (1980) C6-64.
[27] A. Alkauskas, A. Pasquarello, Phys. B 401–402 (2007) 546–549.
[28] K. Matsunaga, Phys. Rev. B 77 (2008) 104106.
[29] M.C. Tarun, M.D. McCluskey, J. Appl. Phys. 109 (2011) 063706.
[30] H. Park, W. Choi, J. Phys. Chem. B 107 (2003) 3885–3890.
[31] J.S. Wang, S. Yin, Q.W. Zhang, F. Saito, T. Sato, J. Mater. Chem. 13 (2003) 2348–2352.
[32] T. Endo, T. Kobayashi, T. Sato, M. Shimada, J. Mater. Sci. 25 (1990) 619–623.
[33] J. Godet, A. Pasquarello, Microelectron. Eng. 84 (2007) 2035–2038.
[34] X. Hu, T. Mohamood, W. Ma, C. Chen, J. Zhao, J. Phys. Chem. B 110 (2006) 26012–26018.
[35] J. Yang, C.C. Chen, H.W. Ji, W.H. Ma, J.C. Zhao, J. Phys. Chem. B 109 (2005) 21900–21907.